A Novel Optimization Design of Dual-Slide Parallel Elastic Actuator for Legged Robots

Liu, Siyu; Ding, Jiatao; Lu, Chunlei; Wang, Zhirui; Su, Bo; Guo, Zhao

DOI
10.1109/TMECH.2024.3401546

Publication date
2024

Document Version
Final published version

Published in
IEEE/ASME Transactions on Mechatronics

A Novel Optimization Design of Dual-Slide Parallel Elastic Actuator for Legged Robots

Siyu Liu, *Graduate Student Member, IEEE*, Jiatao Ding, Chunlei Lu, Zhirui Wang, Bo Su, and Zhao Guo, *Member, IEEE*

***Abstract*—The usage of parallel elastic actuators (PEA) in legged robots could potentially enhance the joints and increase energy efficiency by providing extra torques. However, the current design that adopts tension springs or spiral springs usually requires additional working space for PEA add-ons and enlarges size and mass too much. Besides, they often tune the spring parameters especially the spring constant by hand, failing to achieve optimal performance when considering multiple objectives. To tackle these issues, this article designs a compact dual-slide PEA (DS-PEA) leg that adopts a compression spring structure. Through integrating with a dual-slide mechanism, the PEA elements are attached tightly to the transmission, resulting in a small-size and light-weighted design. Furthermore, we adopt a multiobjective optimization method, i.e., multi-Pareto fronts quantify, to automatically choose the proper spring constant. Simulation and hardware experiments demonstrate that peak torque, motor power, and cost of transport for motion tracking are all largely reduced, even when working at multiple trajectories. Extensive hopping experiments further validate the dynamic motion capability and the energy efficiency of the delicate design. The compact DS-PEA leg will be used in a quadruped robot shortly.**

***Index Terms*—Energy efficiency, hopping, parallel elastic actuator (PEA), stiffness optimization.**

I. Introduction

OVER past few decades, various high-performance legged robots have been developed and employed, such as HRP-5P [1], Mini-Cheetah [2], Walker2 [3]. Compared with these robots, which are driven by rigid actuators (RA), articulated soft-legged robots could reduce energy costs, improve interaction safety, and execute explosive motions, by integrating passive elastic elements in actuation design [4], [5], [6]. According to the mechanical configuration, the current elastic actuators can be divided into series elastic actuation (SEA) [7], [8], [9], where springs serialize the output shaft and payload, and parallel elastic actuation (PEA), where springs are parallelized onto the transmission without changing the integrity of the original mechanism [10], [11]. While both SEA and PEA have their own merits, we focus on the PEA-driven robot.

For PEA design, various types of elastic components can be adopted. Typically, tension spring is used to introduce parallel elastic in linkage transmission [12], [13], leading to a simple structure, without requiring additional guide mechanisms. However, it usually results in nonlinear spring forces/torques [12], inaccurate transmission [13], and an extra working space that leads to low efficiency in space utilization [14]. Apart from it, the spiral springs [15] generate a tangential torque that is more aligned with the direction of the motor torque. Nevertheless, it increases the thickness of the actuator, along with enlarged size and mass. Alternatively, elastic cords offer higher inherent flexibility and interaction safety [16]. However, its complex large-size structure and nonlinearity require careful tuning and optimal design in practical applications.

Aside from mechanical design, the optimization of PEA parameters also needs further investigation. The work in [13] added parallel springs to knee joints of ANYmal robot and optimized the PEA parameter, such as spring constant and rotation diameter in a model-free fashion, which, however, requires heavy computation. The work in [15] optimized the spring characteristics of PEA using a nonparametric method, presenting an analytic result. By modeling the system response, the work in [17] conducted a detailed analysis of the relationship between peak power, energy loss, and PEA frequency. Similarly, Atsushi [12] and Toxiri et al. [16] and considered the characteristics of frequency response and resonance in guiding the robot design. However, they only account for a single metric in optimization formulation and fail to achieve optimal performance when considering multiple task requirements.

To address these issues, we design a novel PEA-driven leg, which adopts compression springs to generate compliant torques. With a delicate dual slide mechanism, the design is lightweight and compact, without increasing the size and mass

Manuscript received 21 January 2024; revised 27 March 2024; accepted 10 May 2024. Date of publication 4 June 2024; date of current version 16 August 2024. Recommended by Technical Editor M. Grebenstein and Senior Editor Q. Zou. This work was supported in part by the National Key Research and Development Program of China under Grant 2023YFE0202100, in part by the National Natural Science Foundation of China under Grant 51605339, and in part by the Collective Intelligence and Collaboration Laboratory (Open Fund Project QXZ23013101). *(Corresponding author: Zhao Guo.)*

Siyu Liu, Chunlei Lu, and Zhao Guo are with the School of Power and Mechanical Engineering, Wuhan University, Wuhan 430072, China (e-mail: guozhao@whu.edu.cn).

Jiatao Ding is with the Department of Cognitive Robotics, Delft University of Technology, 2628, CD Delft, The Netherlands (e-mail: jtdingx@163.com).

Zhirui Wang and Bo Su are with the China North Artificial Intelligence and Innovation Research Institute, and Collective Intelligence and Collaboration Laboratory, Beijing, 100072, China.

This article has supplementary material provided by the authors and color versions of one or more figures available at https://doi.org/10.1109/TMECH.2024.3401546.

Digital Object Identifier 10.1109/TMECH.2024.3401546

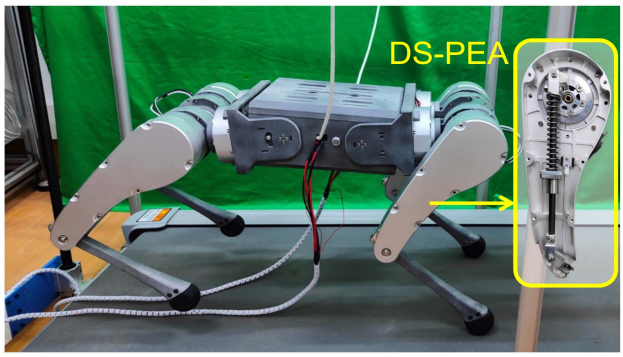

Fig. 1. Quadruped robot with DS-PEA-driven legs.

too much. Furthermore, we introduce an optimization-based approach to automatically choose the optimal PEA parameters. By quantifying multiple Pareto fronts (PFs) [18] for various trajectories, we optimize the parallel elastic when considering multiobjective, including peak torque, power, and energy cost. Finally, we conducted extensive experiments to validate the design reliability, energy efficiency, and the dynamic hopping capacity of the leg with PEA.

An overview of the dual-slide PEA (DS-PEA) leg together with one application in a quadruped robot is illustrated in Fig. 1. Compared with state-of-the-art, our contributions are as follows.

1) A novel *PEA mechanism*. The design with compression springs achieves effective elastic parallel actuation with an extremely small size and low weight.
2) A *multiobjective optimization* algorithm. A modified Pareto optimization helps to obtain the globally optimal spring stiffness under various tasks, trading off peak torque, peak power, and cost of transport (CoT).
3) *Validations* of energetic benefits and dynamic motion capability. Simulations and hardware experiments in multiple scenarios fully evaluate the performance of the DS-PEA leg.

The rest of this article is organized as follows. Section II details the structure and working mechanism of the DS-PEA leg. Section III optimizes the spring stiffness using PFs for the multiobjective method. Section IV validates the performance of DS-PEA. Finally, Section V concludes this article.

II. Mechanical Design

The section details the leg design. We start by introducing the leg structure. Then, we detail the DS-PEA.

A. Overview of Leg Configuration

To simplify the leg structure, we adopt a two-link structure, which is widely used in recent quadruped platforms [2], [19], [20], [21]. As depicted in Fig. 1, the leg comprises three actuated motors, namely, the hip abduction/adduction (HAA), the hip flexion/extension (HFE), and the knee flexion/extension (KFE). The motor is GO-M8010-6, providing a maximum torque of 23 N · m and a maximum speed of 30 rad/s by the gear ratio is 6.33, while maintaining a small size, 96.5 × 92.5 × 42.3 mm and lightweight, 530 g. The range of joints of the leg is shown in Fig. 2(c). To achieve low inertia, we arrange the motors in an adjacent configuration, positioning them in the upper link. Particularly, the hip joint is actuated by the HAA motor attached to the base, followed by the thigh joint, which is actuated by the HFE motor. Then, the calf is actuated by the KFE motor through the 4-bar linkage transmission [see Fig. 2(a)]. To enhance the KFE motor, the DS-PEA, which endows the leg with parallel compliance, is incorporated into the calf transmission. Detailed mechanical parameters of DS-PEA leg are shown in Table I.

TABLE I
Mechanical Parameters of PEA Leg

Joint	Joint limits [°]	Link	length [m]	Mass [kg]
HAA	[-30, 30]	Hip	0.07	0.58
HFE	[-200, 40]	Thigh	0.22	1.48
KFE	[25, 130]	Calf	0.20	0.15
		Foot	0.03	0.03

TABLE II
Comparison of PEA Schemes

PEA schemes	PEA weight/robot [kg]	Extra space
AoPS (ANYmal) [13]	1.2 / 52.5 (2.29%)	Yes
E-GO (GO1) [22]	1.0 / 13.0 (7.69%)	Yes
Frog-inspired robot [14]	0.0083 / 0.1007 (8.24%)	Yes
DS-PEA (ours)	0.196 / 14.3 (1.37%)	No

B. DS-PEA Design

Here, 4-bar linkage transmission is adopted to transmit the motion and force to the knee joint, given its delicate structure, high transmission accuracy, low mass, and low inertia. Particularly, we choose a parallel 4-bar linkage because its one-to-one transmission can simplify the design of link length, as well as kinematics and dynamics. At the same time, the parallel 4-bar linkage is identified as a critical component in the DS-PEA carrier. Then, the DS-PEA is incorporated into this transmission, consisting of a dual-slide mechanism and a compression spring.

As illustrated in Fig. 2(b), the dual-slide mechanism consists of two sliders. Each slider allows sliding along one certain direction, i.e., along vertical and horizontal directions separately. Specifically, the horizontal movement is along the thigh casing while the vertical movement is along the coupler link. The compression spring sleeves over the coupler link, meanwhile, maintain contact with the dual-slide and the input link of the 4-bar linkage. By doing so, the coupler link serves as a guiding mechanism for the compression motion, improving the utilization of the space. The PEA add-ons weigh a total of 49 g, made of aluminum alloy. The comparison of several PEA schemes of legged robots is shown in Table II.

The working mechanism of the DS-PEA is demonstrated by analyzing the status of two positions, namely, the equilibrium position and compression position, as shown in Fig. 2(b). First, we set the spring's equilibrium position to coincide with the lower limit position of the knee joint.[1] From the equilibrium

[1]If the equilibrium position goes beyond the lower limit, the spring would be compressed all the time, resulting in undesired plastic deformation. On the contrary, if the feasible compression stroke is too short, we need to increase the spring stiffness a lot.

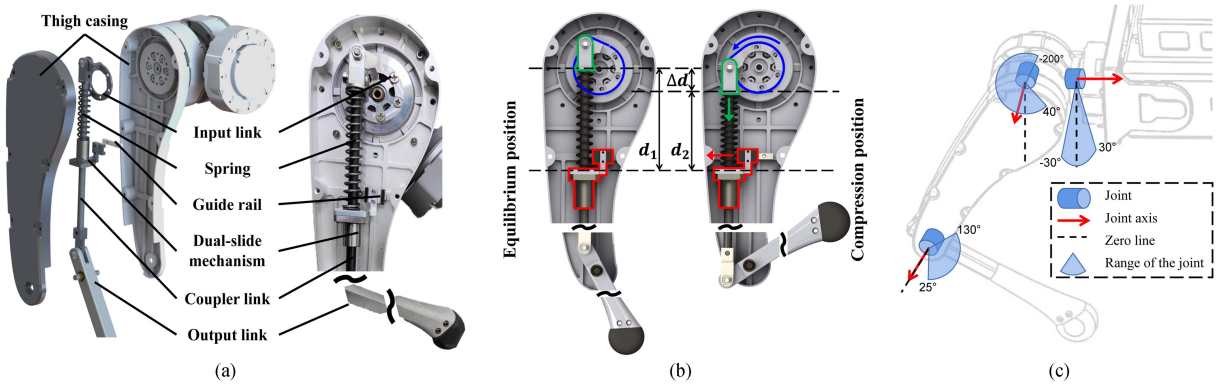

Fig. 2. DS-PEA leg design. (a) Exploded and assembly view. (b) Working mechanism. The black wavy lines represent the omitted length of the thigh and calf to keep an appropriate proportion of the figure. (c) Range of joints of the leg's joints.

TABLE III
DYNAMICS PARAMETERS OF PEA LEG

Parameter	Value	Parameter	Value
l_m [mm]	0.025	m_2 [kg]	0.148
l_1 [mm]	0.220	j_1 [kg×m^2]	0.004
l_2 [mm]	0.230	j_2 [kg×m^2]	0.0003
m_1 [kg]	2.064	r_1, r_2	0.9, 0.2

position to the compression position, the KFE motor [blue circle in Fig. 2(b)] rotates anticlockwise [blue arrow in Fig. 2(b)], and the input link of the 4-bar linkage [green block in Fig. 2(b)] moves downward [green arrow Fig. 2(b)]. However, the height of the dual-slide [red block in Fig. 2(b)] relative to the thigh casing remains constant due to the horizontal movement along the guide rail [red arrow in Fig. 2(b)]. As a result, a change in height difference occurs between the input link and the dual-slide, compressing the spring between the two components and then applying spring force to the input link. Along the force arm, spring torque to the KFE motor and the knee joint is generated. In this case, the storage of elastic potential energy is realized.

III. PARAMETER OPTIMIZATION

To improve the leg performance, it is necessary to optimize the DS-PEA. Particularly, we optimize the elastic component of DS-PEA.[2] Given the equilibrium position in advance, we focus on the spring stiffness optimization.

To obtain the globally optimal spring stiffness, vertically 1-DoF up-down motion is considered, which is the basis of modeling and optimization.

A. Dynamics

As shown in Fig. 3, we restrict the other two degrees of freedom that are separately driven by the HAA motor and HFE motor when modeling the knee joint that DS-PEA actuates. Hence, decoupling the relations of three inner angles of ABC, θ_1, θ_2, θ_3, is shown as (1). In the 1-DoF motion task, the hip is

[2]It is worth mentioning that the usage of a parallel 4-bar line guarantees the 1:1 transmission, alleviating the effort on optimizing the link length and the guide mechanism.

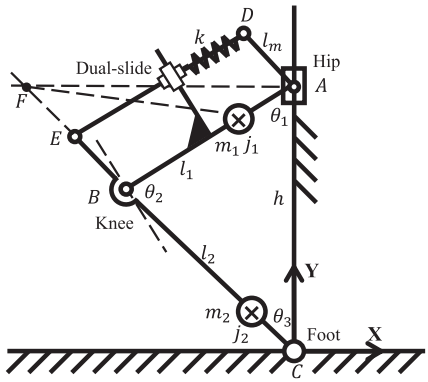

Fig. 3. Modeling of 1-DoF up-down motion.

prismatic to the guide rail through a slider, and the foot is revolute to the ground. The selection of the vertical trajectory is based on the factor that this direction aligns with gravity, allowing for the maximum conversion of gravitational potential energy into elastic potential energy.

$$h = \sqrt{l_1^2 + l_2^2 - 2l_1 l_2 \cos\theta_2}$$
$$\theta_1 = \arcsin\frac{l_2}{h}\sin\theta_2, \theta_3 = \pi - \theta_1 - \theta_2 \tag{1}$$

where h denotes the height of hip relative to the foot and l_1 and l_2 denote the length of the thigh and calf.

An explicit Lagrangian dynamics method is adopted to model the dynamics, where the computation of involved kinetic and potential energies is carried out as follows:

$$L(k, \theta_2, \dot{\theta}_2) = K(\theta_2, \dot{\theta}_2) - U(k, \theta_2)$$
$$\tau(k, \theta_2, \dot{\theta}_2) = \frac{\mathrm{d}}{\mathrm{d}t}\frac{\partial K}{\partial \dot{\theta}_2} - \frac{\partial K}{\partial \theta_2} + \frac{\partial U}{\partial \theta_2} \tag{2}$$

where L denotes the Lagrangian dynamics, K denotes the kinetic energy of DS-PEA leg, U denotes the potential energy of DS-PEA leg, θ_2 denotes the angle of the knee joint, which is equal to the KFE motor output angle, k denotes the spring stiffness, and τ denotes the output torque of KFE motor.

In (2), the kinetic energy of the DS-PEA leg is given by

$$K(\theta_2,\dot{\theta}_2)=\sum_{i=1}^{2}\left(\frac{1}{2}m_i v_i^2+\frac{1}{2}j_i,\omega_i^2\right)$$

$$\boldsymbol{P}_{m_1}=(-l_2\sin\theta_3+r_1l_1\sin\theta_1,l_2\cos\theta_3+r_1l_1\cos\theta_1)$$

$$\boldsymbol{P}_F=(-h\tan\theta_3,h)$$

$$v_1=\dot{\theta}_1|\boldsymbol{P}_{m_1}-\boldsymbol{P}_F|,v_2=\dot{\theta}_3l_2$$

$$\omega_1=\dot{\theta}_1,\omega_2=\dot{\theta}_3 \tag{3}$$

where m_1 and m_2 separately denote the mass of the thigh and calf, v_1 and v_2 separately denote the linear velocity of thigh and calf, j_1 and j_2 separately denote the inertia of thigh and calf, ω_1 and ω_2 separately denote the angular velocity of thigh and calf, $\boldsymbol{P}_{m_1}$ denotes the vector of thigh centroid in the coordinate C, $\boldsymbol{P}_F$ denotes the vector of instantaneous center (F) of the thigh (AB), r_1 and r_2 separately denote the proportion of the centroid to the length of the thigh and calf.

In (2), the potential energy of the DS-PEA leg consists of gravitational potential energy and elastic potential energy. The expression is given by

$$U(k,\theta_2)=U_G(\theta_2)+U_E(k,\theta_2)$$

$$U_G(\theta_2)=\sum_{i=1}^{2}\frac{1}{2}m_igh_i$$

$$U_E(k,\theta_2)=\frac{1}{2}k\Delta l^2$$

$$h_1=l_2\cos\theta_3+r_1l_1\cos\theta_1,h_2=r_2l_2\cos\theta_3$$

$$\Delta l=l_m(\cos(\pi-\theta_0)-\cos(\pi-\theta_2)) \tag{4}$$

where U_G denotes gravitational potential energy, U_E denotes elastic potential energy, g denotes the gravitational acceleration, h_1 and h_2 separately denote the centroid height of thigh and calf in coordinate C, k denotes the spring stiffness of DS-PEA, Δl denotes the amount of spring compression, θ_0 denotes the value of θ_2 when the spring is at its equilibrium position. The dynamics parameters of the PEA leg are listed in Table III.

B. Motion Task

In the vertical motion task, the knee joint moves by following cyclic sine trajectories. Periods and amplitudes of trajectories are taken as parameters to cover multiple occasions. That is, we have the following reference trajectory:

$$\theta_2(t)=A\sin\left(\frac{2\pi}{T}t\right),t\in[0,T] \tag{5}$$

where A and T separately denote the amplitude and period of the reference trajectory, and t is the running time.

Then, the torque on the knee joint [see (2)] is calculated as

$$\tau(k,T,A,t)=\tau(k,\theta_2,\dot{\theta}_2) \tag{6}$$

where $\tau(k,\theta_2,\dot{\theta}_2)$ converts to (6) by subscribing θ_2 and $\dot{\theta}_2$ with (5).

C. Objective Functions

Differing from previous works such as [17], [23], [24] that only focus on one metric, such as peak torque and peak power, we here propose to comprehensively minimize the peak torque, peak power, and mechanical CoT CoT^M [25] with the optimal spring stiffness.

1) *Peak torque* reflects the motor's acuation capability. Reducing the peak torque needed by motors helps to enable the leg to accomplish high-dynamic motions. To this end, we have

$$O_1(k,T,A)=\max(\tau),t\in[0,T] \tag{7}$$

where O_1 denotes the objective function of peak torque.

2) *Peak power* exhibits the motor's power performance. In dynamic motion tasks, merely reducing the peak torque of the KFE motor is not enough due to the conflicts between the motor's output torque and speed. Therefore, we also minimize the peak power, by using

$$O_2(k,T,A)=\max(P^M)=\max(\tau\dot{\theta}_2),t\in[0,T] \tag{8}$$

where O_2 denotes the objective function of peak torque. P^M denotes the mechanical power.

3) CoT^M exhibits the motor's energy efficiency. Reducing CoT^M enables the DS-PEA leg to operate longer and further without enlarging the battery capacity. To this end, we propose to minimize

$$E^M=\int_0^T\tau\dot{\theta}_2\mathrm{d}t,t\in[0,T]$$

$$O_3(k,T,A)=\text{CoT}^M=\frac{E^M}{M_{\text{total}}gS} \tag{9}$$

where E^M denotes the mechanical energy cost of the KFE motor during one period, S denotes the travel distance of the hip, M_{total} denotes the total mass of the leg, O_3 is the objective function of CoT^M.

The rationale for utilizing mechanical outputs as our benchmark, rather than the electrical inputs of the motor, is twofold: First, motors differ a lot from each other, so the mechanical outputs are the more reliable standard. Second, the article's objective is not to design a conventional PEA-actuator but to design a DS-PEA structure tailored for the legged robot. Focusing excessively on the motor's intrinsic features would contradict our initial aims.

D. Optimization Algorithm

In this work, we aim to find the optimal spring stiffness k, which can account for multiple reference trajectories parameterized by T and A. To deal with the multiple objective fictions (defined in Section III-C), we modified the multiple Pareto-front quantify (MPFQ) method [26].

With MPFQ, the optimal stiffness is determined by quantifying the frequency of stiffness occurrence in PFs under arbitrary period and amplitude trajectories. The detailed optimization process is illustrated as pseudocode Algorithm 1.

Algorithm 1: Multi Pareto-Front Quantified.

$n, m, p = 200, 20, 20$
$\boldsymbol{k} = [k_0, \ldots, k_n]$
$\boldsymbol{T} = [T_0, \ldots, T_m]$
$\boldsymbol{A} = [A_0, \ldots, A_p]$
Define: $\mathbf{voxel}[0, \ldots, n][0, \ldots, m][0, \ldots, p][0, 1, 2]$
Define: $\boldsymbol{k}_{quan}[0, 1, \ldots, n][0]$
Step1: Calculate the **voxel**, each $voxel$ has three channels, like red, green, and blue (RGB), separately represent O_1, O_2, O_3
for $i = 1$ to n, $j = 1$ to m, $z = 1$ to p **do**
  $O_1 \leftarrow$ (7) use $\boldsymbol{k}[i], T[j], A[z]$
  $O_2 \leftarrow$ (8) use $\boldsymbol{T}[i], T[j], A[z]$
  $O_3 \leftarrow$ (9) use $\boldsymbol{A}[i], T[j], A[z]$
  $\mathbf{voxel}[i][j][z] \leftarrow (O_1, O_2, O_3)$
end for
Step2: Normalize each channel of all **voxel** to $[0, 1]$
Step3: Find each PF under the given period and amplitude of trajectories
for $j = 1$ to m, $z = 1$ to p, **do**
  $\boldsymbol{k}_p \leftarrow \mathbf{FindPareto}(\mathbf{voxel}[:][\mathbf{j}][\mathbf{z}])$
  for $i = 1$ to n **do**
    if $\boldsymbol{k}[i]$ in $\boldsymbol{k}_p$ **then**
      $\boldsymbol{k}_{quan}[i][0] += 1$
    end if
  end for
end for
Step4: Select the optimal stiffness
$i_{opt} \leftarrow \mathbf{argmax}(\boldsymbol{k}_{quan}[:][0])$
Return $\boldsymbol{k}_{quan}[i_{opt}][0]$

To start, we first choose the boundaries for free variables, i.e., k, A, and T. The spring stiffness ranges from 0 to 9000 N/m, which is commercially accessible. T ranges from 0.5 to 2.0 s, and A ranges from 0.1 to 0.7 m. The k, T, and A are then discretized, formulating vectors given by

$$\begin{aligned} \boldsymbol{k} &= [k_0 \quad k_1 \quad \cdots \quad k_n] \\ \boldsymbol{T} &= [T_0 \quad T_1 \quad \cdots \quad T_m] \\ \boldsymbol{A} &= [A_0 \quad A_1 \quad \cdots \quad A_p] \end{aligned} \tag{10}$$

where $\boldsymbol{k}$, $\boldsymbol{T}$, and $\boldsymbol{A}$ separately denote the vector of stiffness, period, and amplitude sequence. $\boldsymbol{k}$ is discretized into $n = 200$ parts to obtain a more precise globally optimal stiffness. $\boldsymbol{T}$ and $\boldsymbol{A}$ are separately discretized into $m = 20$ and $p = 20$ for generating multiple reference trajectories.

Then, the MPFQ runs as follows.

Step 1. Objective functions computing: Here, the voxel is adopted to visualize the relationship between variables k, T, A and optimization functions O_1, O_2, O_3. In particular, voxel is a 4-dimensional matrix, which is given by

$$\mathbf{voxel} = \mathrm{V}(O_1, O_2, O_3) \tag{11}$$

where $\mathrm{V}(\cdot)$ computes the voxel value, which is a function of (O_1, O_2, O_3) pair. (O_1, O_2, O_3) are computed by Section III-C, given a group of k, A, and T.

Step 2. Voxel normalization: We normalize the values of each optimization function between $[0, 1]$ to prevent one from dominating the others. Note that by doing this, we alleviate the need to adjust weights among different objective functions.

Step 3. PF evaluation: PF, defined as the set of choices, i.e., spring stiffness, upon which no further improvements can be made, is adopted to find the optionally optimal stiffness under a given trajectory. The PF (denoted as k_p) is given by

$$\begin{aligned} k_p = \{k_i \mid \nexists\, k_j \; & O_1(k_j, T, A) \le O_1(k_i, T, A) \\ & O_2(k_j, T, A) \le O_2(k_i, T, A) \\ & O_2(k_j, T, A) \le O_1(k_i, T, A) \\ & \wedge (O_1(k_j, T, A), O_2(k_j, T, A), O_3(k_j, T, A)) \\ & \neq (O_1(k_i, T, A), O_2(k_i, T, A), O_3(k_i, T, A))\} \\ & k_i, k_j \in \boldsymbol{k}, T \in \boldsymbol{T}, A \in \boldsymbol{A} \end{aligned} \tag{12}$$

where k_p is the PF of stiffness under the given period and amplitude.

For more details on PF calculation, please refer to [18].

Step 4. Stiffness determination: Through calculating the frequency of each stiffness in k_ps under all combinations of T and A, we can then select the optimal stiffness with the highest frequency.

IV. Evaluations

This section evaluates the performance of the PEA leg. First, we detail the optimization process in Section III-D, finding the optimal spring stiffness accommodating for the structure parameters. Then, 1-DoF cyclic up-down motion is conducted in simulations and prototype experiments, verifying the improvements brought by DS-PEA in terms of the KFE motor outputs and electricity inputs. Finally, we demonstrate the explosive hopping capability via comparison hardware tests.

A. Optimization Results

Following *Step 1* in Section III-D, calculate the voxels using the dynamics model when given certain parameters including k, A and T. Then, the normalized voxels (Step 2) corresponding to the whole parameters space are obtained [see Fig. 4(a)]. Using Step 3, the PF of a given trajectory is computed. Fig. 4(b) plots the results of three groups of periods and amplitudes, while in the actual optimization, every combination of T and A is taken into account. Based on this, the frequencies of each spring stiffness k is PFs are computed (Step 4), plotted by Fig. 4(c). As can be seen, 5246 N/m holds the highest frequency, which is the optimal result obtained by MPFQ. To directly show the optimal spring stiffness, Fig. 4(d) illustrates the values of three optimization functions under all combinations of trajectories periods and amplitudes with five given stiffnesses, including the optimal stiffness. The closer the color cluster is to the coordinate

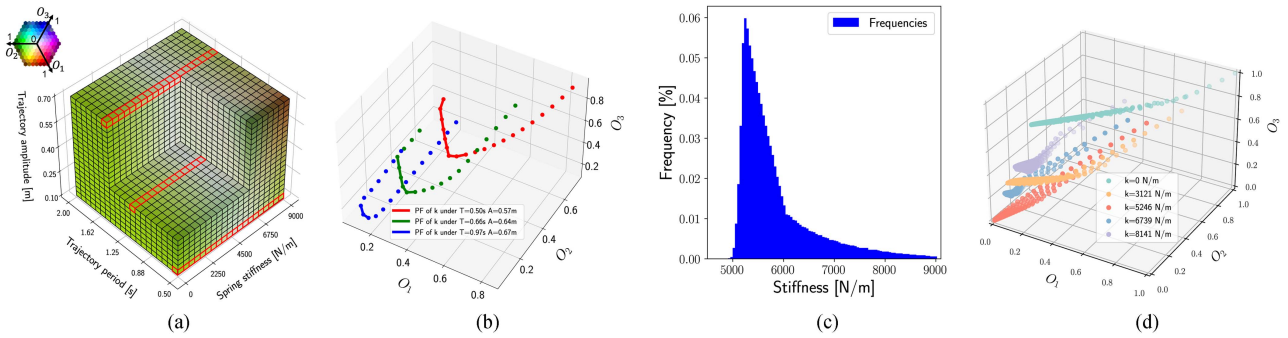

Fig. 4. Optimization results. Voxels in (a) cross-sectional view of optimization functions, each voxel's three channels of RGB represent the values, ranging from 0 to 1. The stiffness under any given trajectory [highlighted by the red box in (a)] is optimized using pareto optimization. (b) Three demos, where each color of the scatters represents the stiffness under the same trajectory, and the line represents the PF for that trajectory. (c) Frequency of each stiffness appearing in the PFs across all trajectories. The color of the scatters of (d) different stiffness. Each color cluster shows the values of three objective functions under all combinations of trajectory periods and frequencies for the given stiffness.

TABLE IV
REDUCTION IN PEAK τ, PEAK P^M, AND CoT^M FROM DYNAMICS MODEL AND SIMULATION

Period [s]	Dynamics model			Simulation		
	Peak τ [Nm]	Peak P^M [W]	CoT^M	Peak τ [Nm]	Peak P^M [W]	CoT^M
0.5	6.61 (54.90%)	30.54 (60.72%)	0.82 (40.98%)	5.50 (46.43%)	30.97 (62.29%)	0.80 (40.40%)
1.0	4.81 (82.20%)	10.68 (70.09%)	1.45 (79.91%)	4.73 (84.77%)	10.78 (74.64%)	1.40 (82.61%)
1.5	3.68 (78.01%)	6.47 (69.22%)	1.43 (78.96%)	3.62 (79.99%)	6.53 (72.64%)	1.40 (80.23%)
2.0	3.22 (74.76%)	4.70 (68.19%)	1.40 (77.46%)	3.20 (76.32%)	4.75 (71.37%)	1.37 (78.14%)

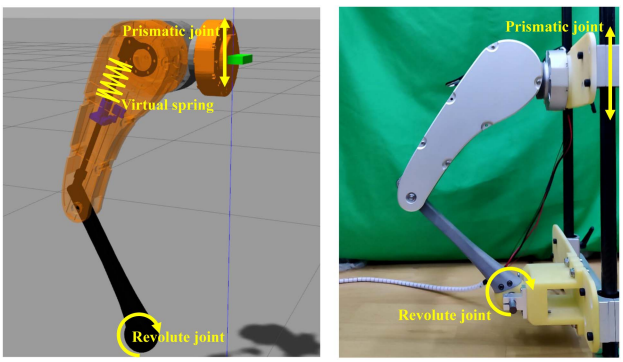

Fig. 5. 1-DoF up-down motion setup of (a) simulation and (b) prototype.

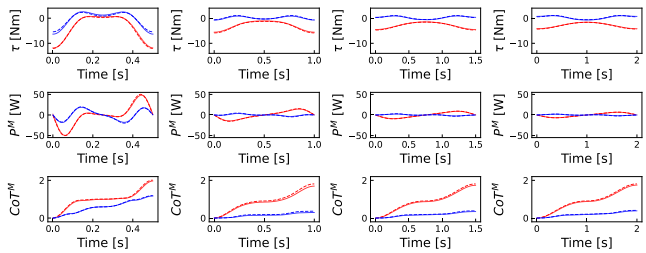

Fig. 6. Results from dynamics model and simulation.

(0, 0, 0), the more optimal the selection of stiffness. The stiffness of 5246 N/m shows its advantage clearly.

B. Simulated 1-DoF Up-Down Performance

Gazebo [27], an open dynamics engine that supports the emulation of open-loop and closed-loop mechanisms, is chosen to simulate our DS-PEA leg. A prismatic joint with adjustable stiffness is employed as the virtual spring of DS-PEA, illustrated on the left side in Fig. 5.

Consistent with the dynamics model in Section III-A and the tasks in Section III-B, the KFE motor tracks the reference sinusoidal trajectory. To validate the performance, multiple simulations are conducted following different trajectories, of which the period T ranges from 0.5 to 2 s and the amplitude A is 0.7 rad.[3] We then recorded the output torques of the KFE motor with RA and DS-PEA. Furthermore, three optimization functions, i.e., O_1, O_2, and O_3, are calculated to highlight the performance improvement brought by DS-PEA. Fig. 6 shows the output torque, power, and CoT^M obtained from the dynamics model and Gazebo physics engine. Table IV quantitatively displays the amount and percentage of reduction.

In the torque graph (the first row of Fig. 6), the output torque of KFE motor with DS-PEA fluctuates around 0 N · m, reaching the expectation that the stiffness of DS-PEA is appropriately optimized. That is, the spring stiffness is neither too small to provide most of the torque required for motion, nor too large to require additional torque to overcome the spring force. When tracking the trajectory with 0.5 s as its period (the first picture in the first row), the DS-PEA leg performs under the support of spring force, where the peak torque is reduced by around 50%, the peak power is reduced by about 60%, and the CoT^M is reduced by about 40%, as illustrated in Table IV. In addition, when the trajectory period ranges from 1.0 to 2.0 s, the

[3]With this amplitude, the robot reaches the joint limits in each test

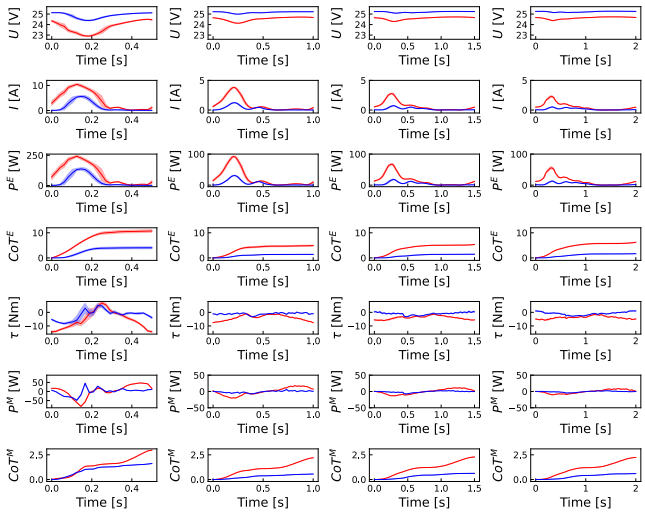

Fig. 7. Mean values and stds. of electrical inputs and mechanical outputs from multiple prototype experiments, tracking 1-DoF up-down trajectories.

abovementioned three optimization objectives are all reduced significantly in summary. And, the percentages of reductions initially increase and then decrease, conforming to the voxel shown in Fig. 4(a) and matching the features of the system's resonance frequency [12].

C. 1-DoF Up-Down Motion in Hardware

This section validates the performance improvements brought by the DS-PEA through the prototype experiments, the same trajectories tasks with Section IV-B. During the hardware experiments, measurements are taken not only of the mechanical outputs but also of the electrical inputs to assess the metrics of extensive parameters. A PD controller is utilized for trajectory tracking.

The electrical input parameters, including input voltage and current of the KFE motor, are measured through the sensors, which have a sampling frequency of 50 Hz, accuracy of 0.2%, and linearity of 0.1%. The mechanical output parameters, including output torque and angles of the KFE motor, are obtained through the internal field oriented control (FOC) current of the motor and rotary encoders. It is worth mentioning that the measured torque calculated by the internal FOC current may not be completely accurate in quantity. However, the trend can still serve as a useful reference. To provide a straightforward comparison, the prototype experiment also conforms to the simulation setup. For each scenario, the leg continuously tracks the trajectory 30 times.

The mean values and the corresponding standard errors (stds.) of electrical input and mechanical output are presented in Fig. 7. The reductions are listed in Table V. The expressions of electrical inputs are given by

$$P^E = \mathrm{UI}$$

$$\mathrm{CoT}^E = \frac{\int_0^T P^E \mathrm{d}t}{M_{\mathrm{total}} g S}, t \in [0, T] \tag{13}$$

TABLE V
REDUCTION IN ELECTRICAL INPUTS AND MECHANICAL OUTPUTS FROM PROTOTYPE EXPERIMENTS

Period [s]	Peak current [A]	Peak P^E [W]	CoT^E
0.5	4.82 (46.29%)	104.69 (43.31%)	6.70 (62.47%)
1.0	2.60 (67.94%)	61.77 (66.81%)	3.52 (71.80%)
1.5	2.03 (73.28%)	48.81 (72.40%)	3.89 (72.89%)
2.0	1.75 (77.13%)	42.37 (76.43%)	4.54 (73.16%)
Period [s]	Peak torque [Nm]	Peak P^M [W]	CoT^M
0.5	5.98 (41.94%)	33.64 (40.84%)	1.35 (45.56%)
1.0	4.50 (58.51%)	13.23 (64.96%)	1.65 (74.94%)
1.5	2.78 (46.17%)	5.76 (43.75%)	1.65 (72.66%)
2.0	2.87 (50.17%)	4.98 (49.35%)	1.63 (73.23%)

where P^E denotes the electrical power, U and I denote the measured voltage and current, and CoT^E denotes the electrical CoT.

Electrical inputs can be seen from Table V and Fig. 7, as the trajectory period increases, the reduction in peak current decreases from 4.82 A (when following the trajectory with the 0.5 s as its period) to 1.75 A (following the trajectory using the 2.0 s as its period), but the percentage decreases increases from 46.29% to 77.13%. The trends of the electrical power P^E and current are similar due to the constant voltage supply. Differing from the current variation, CoT^E always drops a lot, no matter what kind of trajectory is used. Particularly, the reduction percentage reaches 62.47% under 0.5 s trajectory, while more than 70% from 1.0 to 2.0 s. Considering the amount of CoT^E reduction, it reaches 6.7 under the period of 0.5 s while 3.52–4.54 from 0.5 to 2.0 s period.

Mechanical outputs can be seen from Table V and Fig. 7. The trends and reduction amount of output torque, mechanical power and CoT^M are similar to the dynamics and simulation. However, the reduction percentage is a little smaller due to the prototype experiments requiring more mechanical output due to the friction, damping, and maybe-inaccurate FOC current measurements of the platform.

D. Hopping Experiments

Extensive hopping experiments are conducted to validate the dynamic motion capabilities of the DS-PEA leg, as well as the energetic benefits. The reference trajectory, shown in Fig. 8, is generated by the spring-loaded inverted pendulum model [22] and the virtual model control [28] is used for motion tracking. The desired hopping height is 0.5 m, and the leg with/without PEA hopped 5 times. Particularly, we consider two consecutive hops in each trial, consisting of a warm-up hopping, an explosive hopping and a landing. The resultant current, torque, electrical power, and energy cost[4] are shown as Fig. 9, and the values are analyzed in Table VI.

Mentioned as Section IV-C, the output torque is not accurate enough. So we mainly analyze the electrical parameters in this hopping experiment. The torque values can be both positive and negative when DS-PEA is engaged, while the torque values are

[4]When hopping in place, it is difficult to define CoT. Therefore, we analyze the energy cost in this scenario.

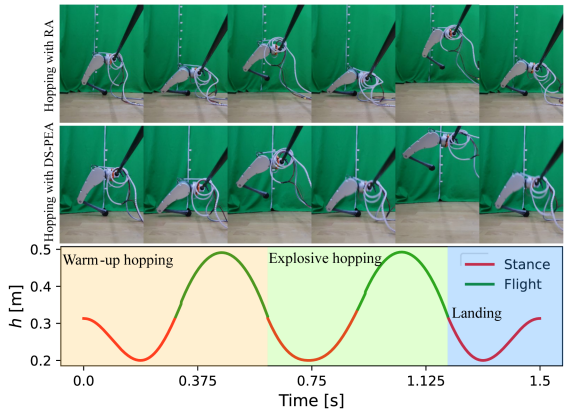

Fig. 8. Prototype hopping experiments. Hopping with RA (top). Hopping with DS-PEA (middle). The reference trajectory (bottom), in which h is the height of the hip relative to the foot.

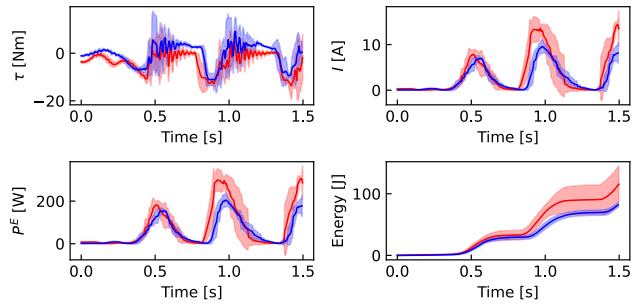

Fig. 9. Comparison between RA and PEA in hopping experiments.

TABLE VI
REDUCTION OF KEY PARAMETERS IN HOPPING EXPERIMENTS

Parameters	Quantity of reduction	Percentage of reduction
Peak τ	2.63 Nm	19.21%
Peak current	4.76 A	33.21%
Peak P^E	100.87 W	33.00%
Input energy	33.48 J	29.00%

almost exclusively negative in the RA case. The analysis shows that the peak torque reduces 19.2%.

During the first warm-up hopping phase, the currents for both RA and DS-PEA are found to be similar. However, during the subsequent explosive hopping and landing phase, a significant reduction in current is observed for DS-PEA, as a result of its energy conversion and impact absorption capabilities. Specifically, peak current, peak power, and the total energy cost were all reduced, by approximately 33.21%, 33.00%, and 29.00%, separately. DS-PEA intervention has led to less fluctuation in data, marked by reduced stds.

V. CONCLUSION

This article presents a novel leg design with parallel compliance, aiming to enhance the joints and increase energy efficiency in robot locomotion. The design utilizes a compression spring structure to provide compliance and adopts a dual-slide mechanism to attach the PEA elements tightly to the transmission link, resulting in a compact and lightweight design. In addition, a multiobjective optimization method is adopted to choose the optimal spring constant, considering the peak torque, peak power, and energy cost. The simulation and prototype experiments demonstrate that the proposed design significantly reduces peak torque, motor power, and energy cost, even with multiple reference trajectories. The delicate design is further validated by extensive hopping experiments, which demonstrate its dynamic motion capability and energy efficiency. The results of this article contribute to the growing field of the compliant robots and offer a promising solution for enhancing the performance of robots in various applications. In the future, we will focus on the controller design of the DS-PEA-driven leg. Another ongoing work is to apply it to legged robots, including quadrupeds and humanoids.

REFERENCES

[1] K. Kaneko et al., "Humanoid robot HRP-5P: An electrically actuated humanoid robot with high-power and wide-range joints," *IEEE Robot. Autom. Lett.*, vol. 4, no. 2, pp. 1431–1438, Apr. 2019.
[2] B. Katz, J. Di Carlo, and S. Kim, "Mini cheetah: A platform for pushing the limits of dynamic quadruped control," in *Proc. IEEE Int. Conf. Robot. Autom.*, 2019, pp. 6295–6301.
[3] J. Ding, T. L. Lam, L. Ge, J. Pang, and Y. Huang, "Safe and adaptive 3-D locomotion via constrained task-space imitation learning," *IEEE/ASME Trans. Mechatron.*, vol. 28, no. 6, pp. 3029–3040, Dec. 2023.
[4] M. Hutter et al., "Anymal—A highly mobile and dynamic quadrupedal robot," in *Proc. IEEE/RSJ Int. Conf. Intell. Robots Syst.*, 2016, pp. 38–44.
[5] A. Badri-Spröwitz, A. Aghamaleki Sarvestani, M. Sitti, and M. A. Daley, "Birdbot achieves energy-efficient gait with minimal control using avian-inspired leg clutching," *Sci. Robot.*, vol. 7, no. 64, 2022, Art. no. eabg4055.
[6] A. R. McN, "Three uses for springs in legged locomotion," *Int. J. Robot. Res.*, vol. 9, no. 2, pp. 53–61, 1990.
[7] N. Kashiri et al., "CENTAURO: A hybrid locomotion and high power resilient manipulation platform," *IEEE Robot. Autom. Lett.*, vol. 4, no. 2, pp. 1595–1602, Apr. 2019.
[8] W. Zhao, J. Liao, W. Qian, H. Yu, and Z. Guo, "A novel design of series elastic actuator using tensile springs array," *Mechanism Mach. Theory*, vol. 192, 2024, Art. no. 105541.
[9] M. Hutter, C. Gehring, M. Bloesch, M. A. Hoepflinger, C. D. Remy, and R. Siegwart, "Starleth: A compliant quadrupedal robot for fast, efficient, and versatile locomotion," in *Adaptive Mobile Robotics*. Singapore: World Scientific, 2012, pp. 483–490.
[10] Z. Ren, W. Roozing, and N. G. Tsagarakis, "The eLeg: A novel efficient leg prototype powered by adjustable parallel compliant actuation principles," in *Proc. IEEE-RAS 18th Int. Conf. Humanoid Robots*, 2018, pp. 1–9.
[11] X. Liu, A. Rossi, and I. Poulakakis, "Spear: A monopedal robot with switchable parallel elastic actuation," in *Proc. IEEE/RSJ Int. Conf. Intell. Robots Syst.*, 2015, pp. 5142–5147.
[12] A. Kakogawa, S. Jeon, and S. Ma, "Stiffness design of a resonance-based planar snake robot with parallel elastic actuators," *IEEE Robot. Autom. Lett.*, vol. 3, no. 2, pp. 1284–1291, Apr. 2018.
[13] F. Bjelonic et al., "Learning-based design and control for quadrupedal robots with parallel-elastic actuators," *IEEE Robot. Autom. Lett.*, vol. 8, no. 3, pp. 1611–1618, Mar. 2023.
[14] C. Hong, D. Tang, Q. Quan, Z. Cao, and Z. Deng, "A combined series-elastic actuator & parallel-elastic leg no-latch bio-inspired jumping robot," *Mechanism Mach. Theory*, vol. 149, 2020, Art. no. 103814.
[15] L. F. Van Der Spaa, W. J. Wolfslag, and M. Wisse, "Unparameterized optimization of the spring characteristic of parallel elastic actuators," *IEEE Robot. Autom. Lett.*, vol. 4, no. 2, pp. 854–861, Apr. 2019.
[16] S. Toxiri, A. Calanca, J. Ortiz, P. Fiorini, and D. G. Caldwell, "A parallel-elastic actuator for a torque-controlled back-support exoskeleton," *IEEE Robot. Autom. Lett.*, vol. 3, no. 1, pp. 492–499, Jan. 2018.
[17] T. Verstraten, P. Beckerle, R. Furnémont, G. Mathijssen, B. Vanderborght, and D. Lefeber, "Series and parallel elastic actuation: Impact of natural dynamics on power and energy consumption," *Mechanism Mach. Theory*, vol. 102, pp. 232–246, 2016.

[18] K. Deb and H. Gupta, "Searching for robust pareto-optimal solutions in multi-objective optimization," in *Proc. Int. Conf. Evol. Multi-Criterion Optim.*, 2005, pp. 150–164.
[19] G. Bledt, M. J. Powell, B. Katz, J. Di Carlo, P. M. Wensing, and S. Kim, "Mit cheetah 3: Design and control of a robust, dynamic quadruped robot," in *Proc. IEEE/RSJ Int. Conf. Intell. Robots Syst.*, 2018, pp. 2245–2252.
[20] P.-A. Léziart, T. Flayols, F. Grimminger, N. Mansard, and P. Souères, "Implementation of a reactive walking controller for the new open-hardware quadruped solo-12," in *Proc. IEEE Int. Conf. Robot. Autom.*, 2021, pp. 5007–5013.
[21] U. Robotics, "Unitree robot go1," 2021. [Online]. Available: https://m.unitree.com/products/go1
[22] J. Ding, M. A. van Löben Sels, F. Angelini, J. Kober, and C. Della Santina, "Robust jumping with an articulated soft quadruped via trajectory optimization and iterative learning," *IEEE Robot. Autom. Lett.*, vol. 9, no. 1, pp. 255–262, Jan. 2024.
[23] W. Roozing, Z. Ren, and N. G. Tsagarakis, "Design of a novel 3-DoF leg with series and parallel compliant actuation for energy efficient articulated robots," in *Proc. IEEE Int. Conf. Robot. Autom.*, 2018, pp. 6068–6075.
[24] D. F. Häufle, M. Taylor, S. Schmitt, and H. Geyer, "A clutched parallel elastic actuator concept: Towards energy efficient powered legs in prosthetics and robotics," in *Proc. IEEE RAS EMBS 4th Int. Conf. Biomed. Robot. Biomechatronics*, 2012, pp. 1614–1619.
[25] H. C. Doets, D. Vergouw, H. E. Veeger, and H. Houdijk, "Metabolic cost and mechanical work for the step-to-step transition in walking after successful total ankle arthroplasty," *Hum. Movement Sci.*, vol. 28, no. 6, pp. 786–797, 2009.
[26] P. Ngatchou, A. Zarei, and A. El-Sharkawi, "Pareto multi objective optimization," in *Proc. 13th Int. Conf. Intell. Syst. Appl. Power Syst.*, 2005, pp. 84–91.
[27] A. Farley, J. Wang, and J. A. Marshall, "How to pick a mobile robot simulator: A quantitative comparison of coppeliasim, gazebo, morse and webots with a focus on accuracy of motion," *Simul. Modelling Pract. Theory*, vol. 120, 2022, Art. no. 102629.
[28] M. Focchi, A. Del Prete, I. Havoutis, R. Featherstone, D. G. Caldwell, and C. Semini, "High-slope terrain locomotion for torque-controlled quadruped robots," *Auton. Robots*, vol. 41, pp. 259–272, 2017.

Siyu Liu (Graduate Student Member, IEEE) received the B.S. degree in mechanical engineering in 2021 from the Wuhan University of Technology, Wuhan, China. He is currently working toward the Ph.D. degree in mechanical engineering with Wuhan University, Wuhan, China.

His research interests mainly focus on legged robots.

Jiatao Ding received the B.Eng. and Ph.D. degrees in engineering from Wuhan University, Wuhan, China, in 2014 and 2020, respectively.

He was a Ph.D. fellow with the Italian Institute of Technology, Genova, Italy, and an Assistant Research Scientist with the Shenzhen Institute of Artificial Intelligence and Robotics for Society, Shenzhen, China. He is currently a Postdoctoral Researcher with the Department of Cognitive Robot, Delft University of University, Delft, The Netherlands. His research interests include locomotion control, imitation learning, and model predictive control.

Chunlei Lu received the B.S. degree in mechanical engineering in 2023 from Wuhan University, Wuhan, China, where he is currently working toward the M.S. degree in mechanical engineering.

Zhirui Wang received the Ph.D. degree in mechanical engineering from Beijing Jiaotong University, Beijing, China, in 2019.

From 2019 to 2022, he was with the China North Vehicle Research Institute, Beijing, China, as an Associate Researcher. Since 2022, he has been with the China North Artificial Intelligence and Innovation Research Institute, Beijing, China, where his research includes the design of ground mobile mechanisms and biomimetic structures for legged robots.

Bo Su received the Ph.D. degree in mechanical engineering from the Huazhong University of Science and Technology, Wuhan, China, in 2011.

From 1993 to 2022, he was with the China North Vehicle Research Institute, Beijing, China, where he was a Research Professor. Since 2022, he has been a Chief Engineer with the China North Artificial Intelligence and Innovation Research Institute, Beijing, China. His research focuses on the overall technologies of unmanned ground systems, special operation robots, and biomimetic robots.

Zhao Guo (Member, IEEE) received the Ph.D. degree in mechatronics engineering from the Institute of Robotics, Shanghai Jiao Tong University, Shanghai, China, in 2012.

From 2012 to 2015, he was a Research Fellow with the Department of Biomedical Engineering, National University of Singapore (NUS), Singapore. He is currently an Associate Professor with the School of Power and Mechanical Engineering, Wuhan University, Wuhan, China. His research interests include compliant actuator, exoskeleton design, modeling and control, and physical human–robot interaction. He mainly focuses on the area of rehabilitation robotics.